How to cite: *Angew. Chem. Int. Ed.* **2025**, *64*, e202510092
doi.org/10.1002/anie.202510092

Proton Channels **Hot Paper**

A Molecular Staircase Built from Hydrazide-Linked Pyridines as an Artificial Proton Channel

Jianhe Xu, Yanbin Chen, Jianru Wang, Wenju Chang, Jie Shen, and Huaqiang Zeng**

Abstract: Artificial proton channels exhibiting high selectivity remain largely unexplored, with only two such systems recently reported. Inspired by the DNA duplex's iconic helical structure, we present here a novel strategy for designing a molecular-scale staircase configuration. The resulting molecular staircase (**MS**), predominantly linear in shape, consists of pyridine units linked by hydrazide groups, with backbone rigidity enhanced by intramolecular H-bonding. This **MS** incorporates up to five proton-transporting motifs, demonstrating remarkable efficacy as a proton-conducting channel within lipid bilayer membranes. Our findings indicate that the **MS** exhibits high proton transport activity (EC_{50} of 0.31 mol%, relative to lipids) and significant selectivity for protons, with selectivity values of 160.3 for K^+, 90.5 for Na^+, and 3.5 for Cl^-. These results underscore the potential of the **MS** and its variants as a highly selective and efficient proton channel, advancing the field of artificial ion transport systems.

The transmembrane transport of ions and large molecules across the hydrophobic barrier of phospholipid bilayers is fundamentally constrained, requiring specialized membrane transport proteins. These proteins facilitate the efficient passage of substances via channel-mediated or carrier-assisted mechanisms,[1–7] overcoming the energetic and structural barriers of the membrane's hydrophobic core.

Proton channels, in particular, play a pivotal role in a multitude of biological processes, including cellular energy production, pH regulation, and signal transduction.[6,7] Proton gradients across cellular membranes are vital for ATP synthesis within mitochondria and for the maintenance of cellular homeostasis.[8] Artificial proton channels aim to replicate the highly selective, rapid, and efficient proton transport observed in biological systems, offering potential solutions for a wide range of applications from biomedical therapies[6,9,10] to energy materials.[11–13] Despite this promise, the development of effective artificial proton channels remains a significant challenge; to date, only two foldamer-derived channel systems have been reported—by Liu[14] and Zeng[15]—while all other known proton-transporting transporters also transport ions[16–19] or H_2O.[20–25] This stands in stark contrast to the rapid advancement of artificial transmembrane transporters designed for the cross-membrane transport of K^+, Cl^-, and H_2O.[26–46]

The double-helix structure of DNA is often metaphorically depicted as a "helical ladder," with base pairs forming the rungs and the sugar-phosphate backbone acting as the rails.[47,48] This canonical architecture not only provides exceptional stability but also facilitates the transmission of genetic information through the dynamic processes of unwinding and rewinding of the double strands. Inspired by this natural design, we have devised and synthesized a foldamer-based artificial molecular staircase (**MS**), aimed at not only expanding the structural diversities of H-bonded aromatic foldamers but also broadening their functional repertoire for transmembrane transport.[15,24,25,29,46,49–53]

Through systematic quantum calculations of the **MS**, we demonstrate that pyridine rings intricately linked by di-acyl-hydrazide bonds take a linear configuration (Figure 1a,b). The computationally optimized structure (Figure 1b) reveals intermolecular H-bonds that ensure orderly assembly of the molecular units. In the **MS**, the five pyridine rings and three di-acyl-hydrazine bonds collectively constitute the "treads" of the **MS**, with the remaining three hydrazide bonds as the "risers." To ensure that the computed structure in Figure 1b corresponds to a true energy minimum, we computed the relative energies of four alternative conformations **1a**-**1d** of the **MS**'s central pyridine unit, flanked by two hydrazide bonds, by systematically breaking one to six H-bonds (Figure S2). Our computations show that the fully H-bonded conformation **1a** is the most stable and is energetically more stable than all others having broken H-bonds by 5.8, 7.0, and 17.9 kcal mol^{-1}, respectively. Comparative analysis of the fully H-bonded linear structure computed in the gas phase with those incorporating solvent effects (methanol, chloroform, DMSO, THF, and gas) confirms that the **MS** molecule consistently adopts a linear and largely planar configuration, stabilized by the intramolecular hydrogen-bonding network (Figure S3). The hydrophobic length of the MS (37.5 Å; Figure 1a) has been carefully tuned to match the hydrophobic thickness of lipid membranes (~34 Å). To optimize structural orientation and enhance ion transport functionality, we incorporated carboxyl groups[54] at both

[*] J. Xu, Y. Chen, J. Wang, Dr. W. Chang, Prof. Dr. J. Shen, Prof. Dr. H. Zeng
College of Chemistry, Fuzhou University, Fuzhou, Fujian 350116, China
E-mail: ShenJie@fzu.edu.cn
hqzeng@fzu.edu.cn

Additional supporting information can be found online in the Supporting Information section

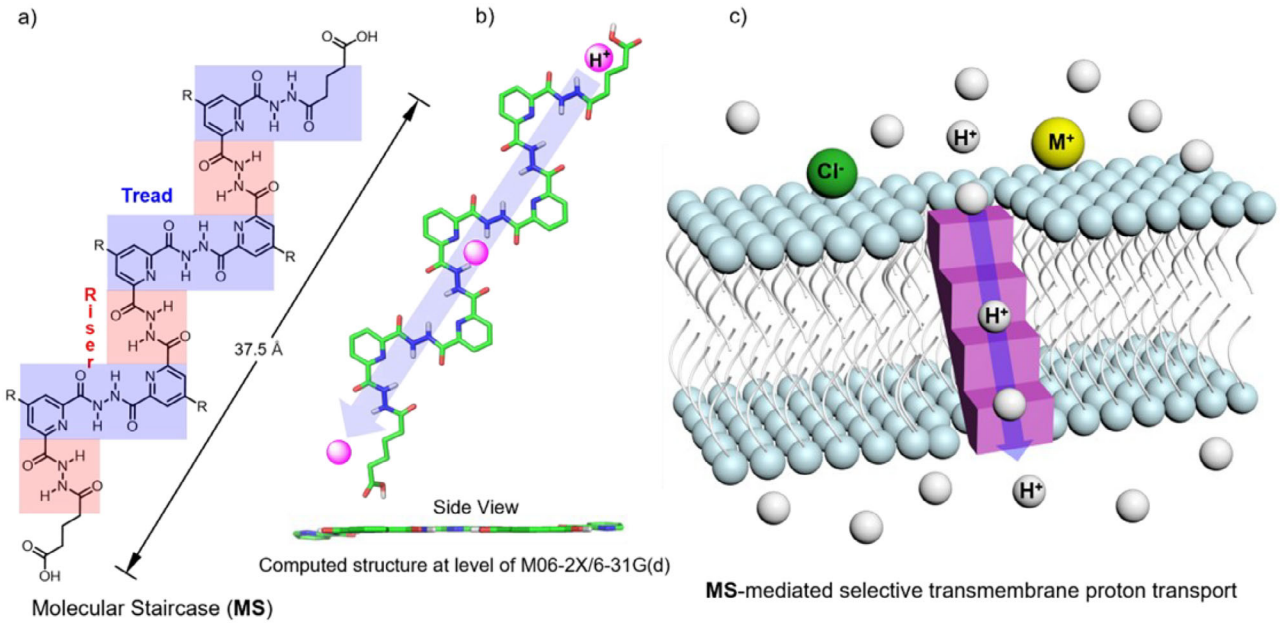

Figure 1. a) Molecular design of molecular staircase **MS**. b) Computationally optimized structure of the **MS** at the m06-2x/6–31G(d) level. c) Schematic illustration of the **MS**-mediated transmembrane proton transport likely via H-atoms of hydrazide bonds or N-atoms of pyridine rings.

ends of the MS to ensure strong attachment of its two ends to the hydrophilic membrane regions, thereby enabling parallel alignment of the **MS** with the hydrocarbon tails of the lipid membrane. The **MS** integrates pyridine groups, along with an abundance of H-bond donors and acceptors. These distinctive structural features are anticipated to confer proton transport capacities when embedded in the membrane (Figure 1c), potentially unlocking new avenues for functional behaviors.

To explore this, we employed the well-established 8-hydroxypyrene-1,3,6-trisulfonic acid trisodium salt (HPTS) assay to evaluate the ion transport activity of the **MS** (Figure 2a). In this assay, HPTS, a pH-sensitive dye, increases in fluorescence as pH rises and was encapsulated within large unilamellar vesicles (LUVs) composed of dioleoylphosphatidylcholine (DOPC) lipids, enabling real-time monitoring of the ion transport process. NaCl (100 mM, pH = 7.0) and MCl (M = Li, Na, K, Rb, and Cs, all at 100 mM, pH = 8.0) buffer solutions were loaded inside and outside the vesicle membrane, respectively, to generate a transmembrane proton gradient.

At a concentration of 2.5 μM, the **MS** exhibits pronounced ion transport activity of 78% in terms of fractional ion transport value and further demonstrates a remarkable independence in activity from the type of MCl (M = Li, Na, K, Rb, and Cs) in the extravesicular environment (Figure 2a). This observation suggests that the **MS** does not facilitate the transport of M^+ ions but instead selectively mediates the transport of H^+, Cl^-, or OH^-, highlighting its specific ion selectivity. Hill analysis reveals an excellent EC_{50} value of 0.32 μM, or 0.33 mol% relative to lipids for the **MS**-mediated transport (Figures 2b and S4). We have further conducted transport experiments in the presence of cholesterol (at a DOPC:cholesterol molar ratio of 2:1) to better simulate the physiological membrane environment (Figure S5). The results show that even at high cholesterol levels, transport activity is reduced by only 10%–15%, suggesting that **MS** may retain comparable performance under biologically relevant conditions.

To elucidate the molecular species transported by the **MS**, we performed two lipid bilayer experiments (Figure 2c,d). Initially, we substituted the 100 mM MCl used in the HPTS assay with 67 mM M_2SO_4 (Figure 2c). Our results reveal that the **MS**-mediated transport activity remained largely unaffected by the type of M_2SO_4, with activity diminishing from 78% for MCl to a range of 46%–52% for M_2SO_4. Given the functional groups present in the **MS**, it is unlikely that the **MS** facilitates the transport of sulfate anions, thereby signifying its proton transport activity. Consequently, the observed decrease in transport efficiency is likely attributable to the significantly reduced membrane permeability of SO_4^{2-} compared to Cl^-, necessary to preserve charge neutrality upon the **MS**-mediated proton efflux.

Subsequently, a chloride-sensitive 6-methoxy-*N*-(3-sulfopropyl)quinolinium (SPQ) dye assay was employed to investigate the **MS**'s capacity for anion transport. SPQ, a fluorescent probe, effectively monitors Cl^- ion transport by exhibiting a decrease in fluorescence intensity as Cl^- concentration increases. In this experiment, vesicles were encapsulated with 0.5 mM SPQ dye and 200 mM $NaNO_3$ at pH 7.0, while the external medium contained 200 mM NaCl at the same pH (Figure 2d). If the **MS** is capable of mediating Cl^- transport, a reduction in SPQ fluorescence intensity would be expected. Indeed, a slight quenching of the SPQ fluorescence was observed at a channel concentration of 2.5 μM. These results indicate that the **MS** exhibits a limited chloride ion transport capacity, further supporting the conclusion that the transport activities observed in the HPTS assay (Figure 2a,c) result from the **MS**'s strong proton transport ability.

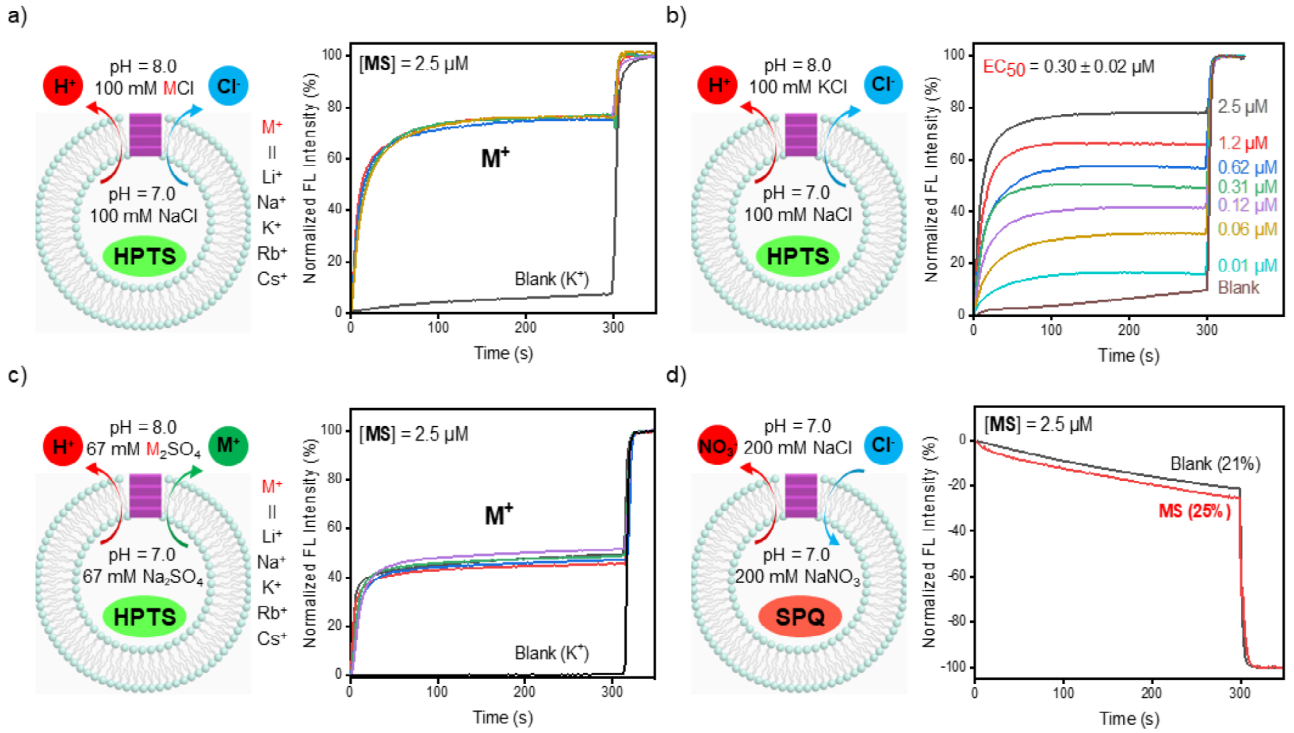

Figure 2. a) The pH-sensitive HPTS assay for assessing ion-transport activities and selectivities of the **MS** in DOPC-based LUVs. b) Hill analysis of the **MS** to determine its EC50 value. c) The HPTS assay with varied extravesicular cations (M_2SO_4) to evaluate the ion transport activity of the **MS**. d) The chloride-sensitive SPQ assay to confirm relatively weak chloride transport activity by the **MS**. HPTS, DOPC, and SPQ. [Total lipids] = 97.5 μM. Triton X-100 was added at 300 s to disrupt the LUVs vesicle, allowing determination of the maximum fluorescence intensity.

To probe proton conductivity of the **MS** at the molecular level, we utilized a planar lipid bilayer membrane made from glyceryl monooleate and cholesterol at a 1:1 molar ratio, as a typical bilayer membrane made from lipid molecules such as DOPC is not stable at high acidity conditions. This membrane configuration has been widely adopted for proton transport studies due to its exceptionally low proton background leakage and outstanding membrane stability under low-pH conditions.[14–15] Single-channel current trace measurements were conducted under symmetric electrolyte conditions (i.e., *cis* chamber = *trans* chamber = 0.25 M HCl, Figures 3a and S6). Under these experimental conditions, we obtained a clear linear relationship in the current–voltage (*I–V*) curve across different applied voltages. Fitting the *I–V* curves yields an Ohmic response, enabling us to determine the proton conductivity (γ_{H^+}) of the **MS** as 15.4 ± 0.7 pS (Figures 3b, S7, and S8). To further assess proton transport selectivity, we recorded single-channel current traces in asymmetric baths (*cis* chamber = 0.25 M HCl and *trans* chamber = 0.10 M HCl) to evaluate the H^+/Cl^- transport selectivity at the single-channel level. Curve fitting provides the reverse potential value of 78.5 mV (ε_{rev}, Figures 3c, S9, and S10). After accounting for the Nernst potential difference arising from the proton gradient of 0.10 to 0.25 M, the reverse potential value was used in the simplified Goldman–Hodgkin–Katz equation (Figure 3c and Supporting Information) to calculate the H^+/Cl^- ion selectivity, yielding a value of 3.5. Similarly, using the ε_{rev} values of 115.5 and 130.4 mV (Figures 3d,e and S11–S16), the H^+/K^+ and H^+/Na^+ ion selectivity values were determined to be 90.5 and 160.3, respectively. While the proton conductance of the **MS** (15.4 pS) is smaller than the values 62.5[14] and 252.6 pS[15] for two recently reported foldamer-based proton channels, its transport efficiency approaches that of the native M2 proton channel protein.[15] In terms of transport selectivity, the **MS** demonstrates its H^+/K^+ selectivity value of 90.5 and H^+/Na^+ value of 160.3, which are comparable to those reported by Yan et al. (74.8 and 225.1, respectively)[14] and our earlier work (81.5 and 122.7).[15] Nevertheless, these selectivity values remain far below the exceptionally high benchmark selectivity of M2 proton channels, which exhibit over 10^5-fold preference for H^+ over other monovalent cations, indicating ample room for further improvement of artificial proton channels.

After demonstrating the **MS**'s ability to selectively transport protons, the remaining question concerns the underlying origin of this ability. It has been established that directionally aligned, consecutive NH groups are integral to mediating proton transport via hydrogen exchange.[14] Considering the abundance of NH groups within the **MS** molecule, we hypothesized that the linear arrangement of these groups could be crucial to facilitating proton transport through a hopping mechanism. To examine this hypothesis further, we investigated the mobility of H-atoms in the NH groups by conducting hydrogen–deuterium (H–D) exchange experiments.

The ^1H NMR spectrum of the **MS** (Figures 4, S17, and S18) reveals four distinct NH groups, categorized as H_a, H_b, and H_c. The H–D exchange experiment was initiated by adding

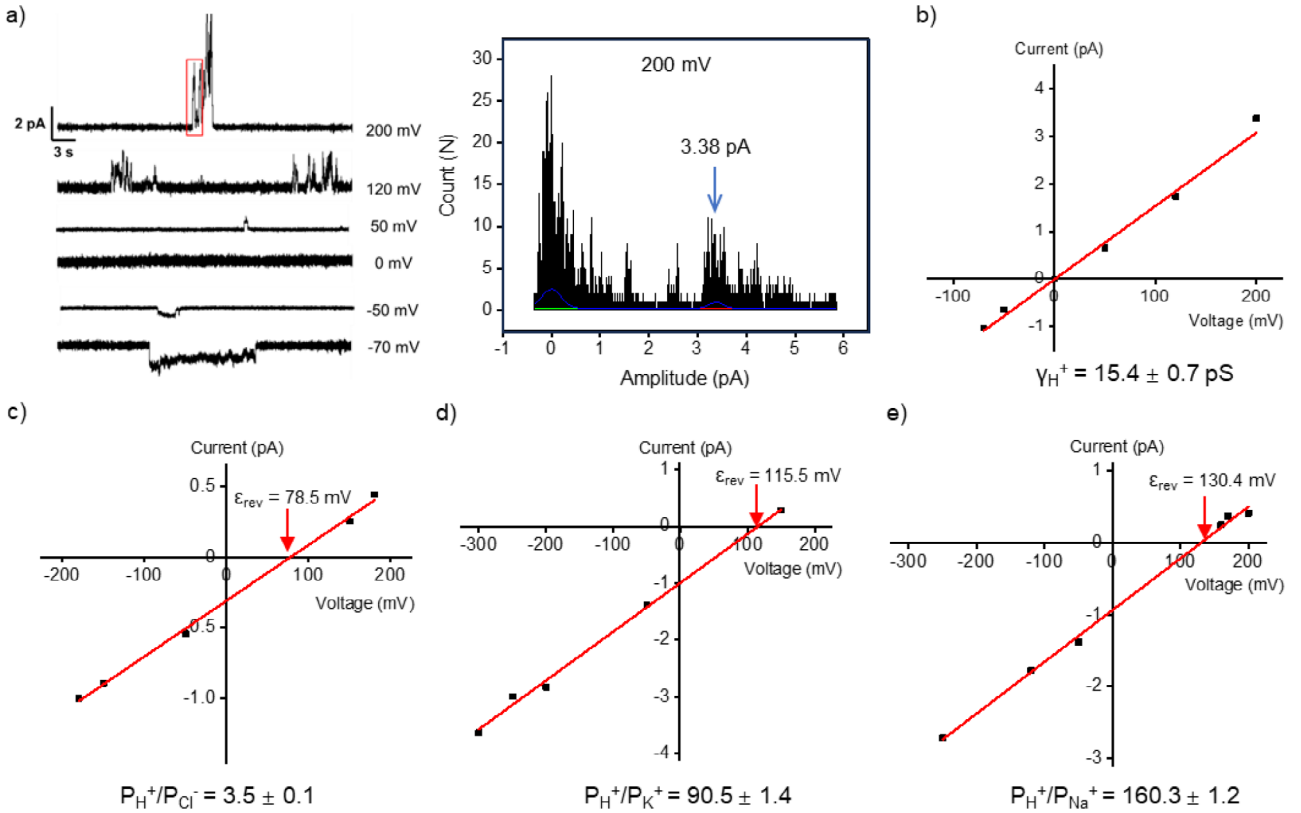

Figure 3. a) Single-channel current traces recorded in symmetric baths (*cis* chamber = *trans* chamber = 0.25 M HCl) for the **MS** and an exemplified point amplitude histogram for the digitized current values that gives a mean value of 3.38 pA at 200 mV. For average current values and histograms at other voltages, see Figures S7 and S8. b) Determination of H^+ conductance (γH^+) for the **MS** using a linear ohmic current–voltage (*I–V*) curve. c) Permeability ratio of P_{H^+}/P_{Cl^-} was obtained by fitting the *I–V* curve using the simplified Goldman–Hodgkin–Katz equation $\varepsilon rev + 23.5 = RT/F \times \ln\{(P_{H^+} \times [H^+]trans + P_{Cl^-}[Cl^-]cis/(P_{H^+} \times [H^+]cis + P_{Cl^-} \times [Cl^-]trans)\}$. For d) and e), the corresponding equation is $\varepsilon rev = RT/F \times \ln(P_{M^+}/P_{H^+})$. Here, 23.5 mV is the Nernst potential corresponding to a proton gradient of 0.10 to 0.25 M, R = universal gas constant (8.314 J•K^{-1}•mol^{-1}), T = 300 K, F = Faraday's constant (96 485 C•mol^{-1}).

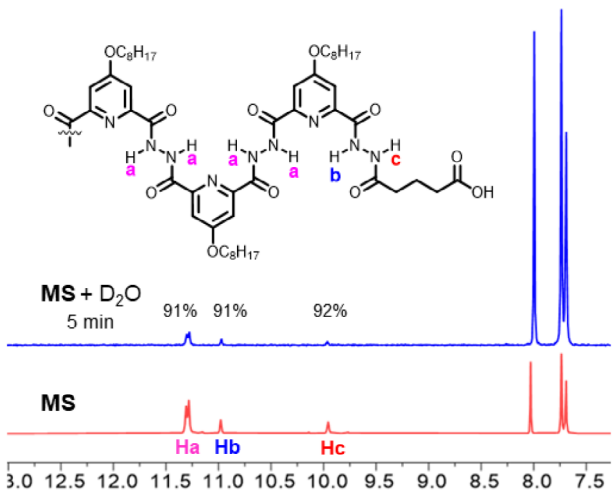

Figure 4. ^{1}H NMR spectra of the **MS** at 2.43 mM a) before and b) after addition of 10 µL D_2O in a mixed solvent (DMSO-d_6 = $CDCl_3$ = 295 µL) at room temperature, showing that more than 90% of the H–D exchange is completed within 5 min. Note that the peaks from 7.5 to 8.1 ppm are not affected by the H–D exchange process.

10 µL of D_2O into a 2.43 mM solution of the **MS** in a mixed solvent (DMSO-d_6 = $CDCl_3$ = 295 µL). Experimental results demonstrate that the H-atoms of all NH groups undergo exchange by more than 90%, indicating rapid and nearly complete H–D exchange within 5 min. These results confirm the highly labile nature of these H-atoms, suggesting their likely involvement as proton-hopping sites that are consistent with early findings.[14] Certainly, pyridine groups or H_2O molecules that bind to the **MS** can also contribute to the proton transport process.

In summary, this work introduces a pioneering foldamer-based staircase structure that mediates proton transport in a highly selective manner, utilizing a hopping mechanism, and demonstrating impressive selectivity values of 160.3 for H^+/Na^+ and 90.5 for H^+/K^+. While the linearly arranged NH groups appear to facilitate proton exchange and hopping within the staircase framework, the precise mechanism underlying proton transport remains to be fully elucidated. When considered alongside the recent advancements in membrane-active molecular machines, which operate through unconventional swing-relaying,[55–58] swinging,[59] fishing,[60] shuttling,[61,62] drilling,[63,64] swimming,[65] and rotating mechanisms,[66] this innovative staircase structure

opens new avenues for the design and construction of artificial channels with novel transport mechanisms, holding promising applications across a spectrum of fields, from nanotechnology and energy to medicine.

Acknowledgements

This work is supported by the National Natural Science Foundation of China (22371048 and 22271049), the " Chu ying Program" for the Top Young Talents of Fujian Province, the Natural Science Foundation of Fujian Province (2023J01054) and a start-up grant from Fuzhou University

Conflict of Interests

The authors declare no conflict of interest.

Data Availability Statement

The data that support the findings of this study are available from the corresponding author upon reasonable request.

Keywords: Molecular staircase • Proton channels • Proton transport • Transmembrane transport

[1] F. H. Yu, W. A. Catterall, *Genome Biol.* **2003**, *4*, 207.
[2] D. A. Doyle, J. M. Cabral, R. A. Pfuetzner, A. Kuo, J. M. Gulbis, S. L. Cohen, B. T. Chait, R. MacKinnon, *Science* **1998**, *280*, 69–77.
[3] H. Reuter, *Nature* **1985**, *316*, 391–391.
[4] R. Dutzler, E. B. Campbell, R. MacKinnon, *Science* **2003**, *300*, 108–112.
[5] J. Guo, W. Zeng, Q. Chen, C. Lee, L. Chen, Y. Yang, C. Cang, D. Ren, Y. Jiang, *Nature* **2016**, *531*, 196–201.
[6] Y. Shen, Y. Luo, P. Liao, Y. Zuo, R. Jiang, *Neurosci. Bull.* **2023**, *39*, 1157–1172.
[7] T. E. DeCoursey, *Annu. Rev. Physiol.* **2024**, *86*, 357–377.
[8] T. Sekiguchi, K. Yoshida, K.-i. Wakabayashi, T. Hisabori, *J. Biol. Chem.* **2024**, *300*, 107659.
[9] Y. Wang, X. Wu, Q. Li, S. Zhang, S. J. Li, *PLoS One* **2013**, *8*, e70550.
[10] H. Pang, X. Wang, S. Zhao, W. Xi, J. Lv, J. Qin, Q. Zhao, Y. Che, L. Chen, S. J. Li, *J. Biol. Chem.* **2020**, *295*, 3601–3613.
[11] K. A. Mauritz, R. B. Moore, *Chem. Rev.* **2004**, *104*, 4535–4585.
[12] H. Qin, H. Wu, S.-M. Zeng, F. Yi, S.-Y. Qin, Y. Sun, L. Ding, H. Wang, *Adv. Membr.* **2022**, *2*, 100046.
[13] J. Lu, H. Xu, H. Yu, X. Hu, J. Xia, Y. Zhu, F. Wang, H.-A. Wu, L. Jiang, H. Wang, *Sci. Adv.* **2022**, *8*, eabl5070.
[14] T. Yan, S. Liu, J. Xu, H. Sun, S. Yu, J. Liu, *Nano Lett.* **2021**, *21*, 10462–10468.
[15] J. Shen, R. Ye, Z. Liu, H. Zeng, *Angew. Chem. Int. Ed.* **2022**, *61*, e202200259.
[16] L. A. Weiss, N. Sakai, B. Ghebremariam, C. Ni, S. Matile, *J. Am. Chem. Soc.* **1997**, *119*, 12142–12149.
[17] M. Barboiu, Y. Le Duc, A. Gilles, P.-A. Cazade, M. Michau, Y. Marie Legrand, A. van der Lee, B. Coasne, P. Parvizi, J. Post, T. Fyles, *Nat. Commun.* **2014**, *5*, 4142.
[18] C. Lang, W. Li, Z. Dong, X. Zhang, F. Yang, B. Yang, X. Deng, C. Zhang, J. Xu, J. Liu, *Angew. Chem. Int. Ed.* **2016**, *55*, 9723–9727.
[19] C. Jia, D. Luo, J. Zhou, X. Xie, H. Yuen In Lam, P. Li, Y. Mu, Z. Zeng, C. Ren, *Angew. Chem. Int. Ed.* **2025**, *64*, e202419800.
[20] W. Si, L. Chen, X.-B. Hu, G. Tang, Z. Chen, J.-L. Hou, Z.-T. Li, *Angew. Chem. Int. Ed.* **2011**, *50*, 12564–12568.
[21] M. Barboiu, A. Gilles, *Acc. Chem. Res.* **2013**, *46*, 2814–2823.
[22] B. Gong, Z. Shao, *Acc. Chem. Res.* **2013**, *46*, 2856–2866.
[23] H. Q. Zhao, S. Sheng, Y. H. Hong, H. Q. Zeng, *J. Am. Chem. Soc.* **2014**, *136*, 14270–14276.
[24] J. Shen, R. J. Ye, A. Romanies, A. Roy, F. Chen, C. L. Ren, Z. W. Liu, H. Q. Zeng, *J. Am. Chem. Soc.* **2020**, *142*, 10050–10058.
[25] J. Shen, J. Fan, R. J. Ye, N. Li, Y. Mu, H. Q. Zeng, *Angew. Chem. Int. Ed.* **2020**, *59*, 13328–13334.
[26] F. Otis, M. Auger, N. Voyer, *Acc. Chem. Res.* **2013**, *46*, 2934–2943.
[27] J. Montenegro, M. R. Ghadiri, J. R. Granja, *Acc. Chem. Res.* **2013**, *46*, 2955–2965.
[28] T. M. Fyles, *Acc. Chem. Res.* **2013**, *46*, 2847–2855.
[29] Y. P. Huo, H. Q. Zeng, *Acc. Chem. Res.* **2016**, *49*, 922–930.
[30] B. Gong, *Faraday Discuss.* **2018**, *209*, 415–427.
[31] H. Gill, M. R. Gokel, M. McKeever, S. Negin, M. B. Patel, S. Yin, G. W. Gokel, *Coord. Chem. Rev.* **2020**, *412*, 213264.
[32] J. T. Davis, P. A. Gale, R. Quesada, *Chem. Soc. Rev.* **2020**, *49*, 6056–6086.
[33] X. Wu, A. M. Gilchrist, P. A. Gale, *Chem* **2020**, *6*, 1296–1309.
[34] S.-P. Zheng, L.-B. Huang, Z. Sun, M. Barboiu, *Angew. Chem. Int. Ed.* **2021**, *60*, 566–597.
[35] J. Yang, G. Yu, J. L. Sessler, I. Shin, P. A. Gale, F. Huang, *Chem* **2021**, *7*, 3256–3291.
[36] K. Sato, T. Muraoka, K. Kinbara, *Acc. Chem. Res.* **2021**, *54*, 3700–3709.
[37] A. Roy, P. Talukdar, *ChemBioChem* **2021**, *22*, 2925–2940.
[38] W. Song, M. Kumar, *Langmuir* **2022**, *38*, 9085–9091.
[39] T. Yan, X. Zheng, S. Liu, Y. Zou, J. Liu, *Sci. China Chem.* **2022**, *65*, 1265–1278.
[40] A. Mondal, M. Ahmad, D. Mondal, P. Talukdar, *Chem. Commun.* **2023**, *59*, 1917–1938.
[41] L. He, T. Zhang, C. Zhu, T. Yan, J. Liu, *Chem. - Eur. J.* **2023**, *29*, e202300044.
[42] M. Ahmad, S. A. Gartland, M. J. Langton, *Angew. Chem. Int. Ed.* **2023**, *62*, e202308842.
[43] J. Shen, C. Ren, H. Q. Zeng, *Acc. Chem. Res.* **2022**, *55*, 1148–1159.
[44] T. G. Johnson, M. J. Langton, *J. Am. Chem. Soc.* **2023**, *145*, 27167–27184.
[45] X. Yuan, J. Shen, H. Q. Zeng, *Chem. Commun.* **2024**, *60*, 482–500.
[46] D. Zhang, W. Chang, J. Shen, H. Q. Zeng, *Chem. Commun.* **2024**, *60*, 13468–13491.
[47] J. D. Watson, F. H. C. Crick, *Nature* **1953**, *171*, 737–738.
[48] M. H. F. Wilkins, A. R. Stokes, H. R. Wilson, *Nature* **1953**, *171*, 738–740.
[49] J. Shen, C. L. Ren, H. q. Zeng, *J. Am. Chem. Soc.* **2017**, *139*, 5387–5396.
[50] H. Q. Zhao, J. Shen, C. L. Ren, W. Zeng, H. Q. Zeng, *Org. Lett.* **2017**, *19*, 2190–2193.
[51] A. Roy, H. Joshi, R. J. Ye, J. Shen, F. Chen, A. Aksimentiev, H. Q. Zeng, *Angew. Chem. Int. Ed.* **2020**, *59*, 4806–4813.
[52] A. Roy, J. Shen, H. Joshi, W. Song, Y.-M. Tu, R. Chowdhury, R. Ye, N. Li, C. Ren, M. Kumar, A. Aksimentiev, H. Q. Zeng, *Nat. Nanotech.* **2021**, *16*, 911–917.
[53] J. Shen, A. Roy, H. Joshi, L. Samineni, R. J. Ye, Y.-M. Tu, W. Song, M. Skiles, M. Kumar, A. Aksimentiev, H. Q. Zeng, *Nano Lett.* **2022**, *22*, 4831–4838.
[54] H.-M. Ren, B.-Y. Liu, B.-T. Zuo, Z.-F. Li, G. Li, *Micropor. Mesopor. Mater.* **2023**, *351*, 112481.

[55] B. A. McNally, E. J. O'Neil, A. Nguyen, B. D. Smith, *J. Am. Chem. Soc.* **2008**, *130*, 17274–17275.
[56] N. Li, F. Chen, J. Shen, H. Zhang, T. Wang, R. Ye, T. Li, T. P. Loh, Y. Y. Yang, H. Q. Zeng, *J. Am. Chem. Soc.* **2020**, *142*, 21082–21090.
[57] T. G. Johnson, A. Sadeghi-Kelishadi, M. J. Langton, *J. Am. Chem. Soc.* **2022**, *144*, 10455–10461.
[58] H. Yang, J. Yi, S. Pang, K. Ye, Z. Ye, Q. Duan, Z. Yan, C. Lian, Y. Yang, L. Zhu, D.-H. Qu, C. Bao, *Angew. Chem. In. Ed.* **2022**, *61*, e202204605.
[59] C. Ren, F. Chen, R. J. Ye, Y. S. Ong, H. Lu, S. S. Lee, J. Y. Ying, H. Q. Zeng, *Angew. Chem. Int. Ed.* **2019**, *58*, 8034–8038.
[60] R. J. Ye, C. L. Ren, J. Shen, N. Li, F. Chen, A. Roy, H. Q. Zeng, *J. Am. Chem. Soc.* **2019**, *141*, 9788–9792.
[61] S. Chen, Y. Wang, T. Nie, C. Bao, C. Wang, T. Xu, Q. Lin, D.-H. Qu, X. Gong, Y. Yang, L. Zhu, H. Tian, *J. Am. Chem. Soc.* **2018**, *140*, 17992–17998.
[62] C. Wang, S. Wang, H. Yang, Y. Xiang, X. Wang, C. Bao, L. Zhu, H. Tian, D.-H. Qu, *Angew. Chem. Int. Ed.* **2021**, *60*, 14836–14840.
[63] V. Garcia-Lopez, F. Chen, L. G. Nilewski, G. Duret, A. Aliyan, A. B. Kolomeisky, J. T. Robinson, G. Wang, R. Pal, J. M. Tour, *Nature* **2017**, *548*, 567–572.
[64] A. L. Santos, D. Liu, A. K. Reed, A. M. Wyderka, A. van Venrooy, J. T. Li, V. D. Li, M. Misiura, O. Samoylova, J. L. Beckham, C. Ayala-Orozco, A. B. Kolomeisky, L. B. Alemany, A. Oliver, G. P. Tegos, J. M. Tour, *Sci. Adv.* **2022**, *8*, eabm2055.
[65] H. Zhang, R. Ye, Y. Mu, T. Li, H. Q. Zeng, *Nano Lett.* **2021**, *21*, 1384–1391.
[66] H. Ma, R. Ye, L. Jin, S. Zhou, C. Ren, H. Ren, J. Shen, H. Q. Zeng, *Chin. Chem. Lett. 34*, 108355.

Manuscript received: May 07, 2025
Revised manuscript received: June 29, 2025
Accepted manuscript online: July 18, 2025
Version of record online: July 29, 2025